Numerical investigation on the thermal-hydraulic performance of supercritical CO_2 in a modified airfoil fins heat exchanger

Zengxiao Han[a,b], Jiangfeng Guo[a,b,c,d,*], Haiyan Liao[e], Zhongmei Zhang[e], Xiulan Huai[a,b,d]

[a]*Institute of Engineering Thermophysics, Chinese Academy of Sciences, Beijing 100190, China*

[b] *School of Engineering Science, University of Chinese Academy of Sciences, Beijing 100049, China*

[c]*Department of Chemical Engineering, Imperial College London, London SW7 2AZ, UK*

[d]*Nanjing Institute of Future Energy System, Nanjing 211135, China*

[e]*GD Power Development Co., LTD. CHN Energy, Beijing 100101, China*

N.B.: This is the accepted version of this article. The final, published version of the article can be found at: https://doi.org/10.1016/j.supflu.2022.105643

Abstract

The numerical studies on the modified airfoil fins channel using supercritical CO_2 as working fluid showed that front-dense and rear-sparse (FDRS) and front-sparse and rear-dense (FSRD) distributions of fins could enhance heat transfer by improving the distribution uniformity of temperature difference in channel. The match of local dense distribution of fins with the region near pseudocritical point could obtain better overall thermal performance in the modified airfoil fins heat exchanger. The differences of thermal-hydraulic performance among channels with uniform, FDRS and FSRD distributions of fins could be explained with field synergy principle. The FSRD distribution of fins is the optimum scheme in the three distributions of the modified airfoil fins channel, because its comprehensive performance is 23 % to 29 % higher than that of the uniform distribution of fins and 2 % to 7.6 % higher than that of the FDRS distribution of fins. The present work provides insights into the mechanisms of supercritical CO_2 heat transfer characteristics as well as practical guidance on the design and optimisation of relevant components.

Keywords: Supercritical CO_2 (SCO_2); modified airfoil fins heat exchanger; distribution optimisation; field synergy principle; thermal-hydraulic performance

1. Introduction

*Corresponding author. *E-mail address*: gjf1200@126.com (J. Guo)

With continuous development of economy and society, improving energy utilization efficiency has become a consensus in the energy utilization field. The supercritical pressure CO_2 Brayton cycle (SCO_2-BC) is an efficient and compact power cycle, which has promising potentials in solar and nuclear power generation systems [1-3]. The printed circuit heat exchanger (PCHE) is an ideal candidate as regenerator and cooler in SCO_2-BC due to its advantages of high compactness and efficiency.

In SCO_2-BC cooler, the thermophysical properties of SCO_2 change drastically along the channel, which affects the prediction of the thermal-hydraulic characteristics of SCO_2 and brings great difficulties to optimise the SCO_2 cooler. Liao et al. [4] found that the traditional correlations cannot predict the heat transfer characteristics of SCO_2 accurately. Thus, the accurate knowledge of thermal-hydraulic characteristics for SCO_2 near the pseudocritical temperature (T_{pc}) and the appropriate optimisation for heat transfer structure are significant to the optimisation of SCO_2 cooler.

The studies about the thermal-hydraulic characteristics of SCO_2 near T_{pc} have attracted lots of attentions. Li et al. [5] concluded that the heat transfer coefficient (h) of SCO_2 reaches its peak when the bulk temperature (T_b) of SCO_2 nears T_{pc} under cooling conditions. Du et al. [6] analysed the thermal-hydraulic performance of SCO_2 in horizontal cooling tube by simulation and found that the thermal performance of SCO_2 is improved as heat flux increases. Dang and Hihara [7,8] found that the influence of heat flux on the thermal performance of SCO_2 is more obvious in the region where T_b of SCO_2 near T_{pc}. Xiang et al. [9] found that the increase of heat flux and hydraulic diameter strengthens the buoyancy effect and heat flux affects the peak position of h in tube. Zhang et al. [10] analysed the thermodynamic properties of SCO_2 in horizontal tubes by numerical simulation. The results indicated that the effective thermal conductivity of SCO_2 affects its local thermal performance. The heat transfer and flow characteristics of SCO_2 in cooling vertical tubes were analysed by Guo et al. [11], the results showed that h reaches its maximum value (h_{peak}) when T_b/T_{pc} is about 1.01.

Besides, the optimisation of heat transfer structures based on the local thermophysical properties of SCO_2 is more beneficial for the performance enhancement of PCHE. A variety of channels have been developed to improve the performance of PCHE, including straight, zigzag, S-shaped fins and airfoil fins channels [12]. The thermal-hydraulic performance of SCO_2 in straight channel with different cross-sections was compared by Jeon et al. [13]. The empirical correlations of semi-circular straight channel were summarized by Kim et al. [14]. The thermal-hydraulic performance of SCO_2 in zigzag channel was investigated by Zhang et al. [15], it was found that the better performance is observed in zigzag channel with zigzag angle between 110° to 130°. Kim et al. [16] explored the influences of hydraulic diameter, zigzag angle and channel pitch on the thermal-

hydraulic performance, and the relevant empirical correlations of zigzag channel were summarized. Serpentine channel and some discontinuous fins channels were proposed to reduce additional pressure drop (ΔP) caused by zigzag channel. Cui et al. [17] analysed the influences of camber, cross-sectional shape and curvature diameter on the comprehensive performance of serpentine channel. The results showed that increasing the camber or reducing the curvature diameter could strengthen comprehensive performance. Ngo et al. [18,19] presented the S-shaped fins channel and compared the thermal-hydraulic performance between S-shaped fins channel and zigzag channel. They reported that the thermal performance of S-shaped fins channel is poorer than that of zigzag channel but the hydraulic performance of the S-shaped fins channel is better than that of zigzag channel. Kim et al. [20] numerically investigated the performance of channel with NACA 0020 airfoil fins, and found that the ΔP in this channel is 1/20 of that in zigzag channel. Chen et al. [21] reported that the thermal performance of channel with airfoil fins increases as fins thickness increases. The effect of the distribution of airfoil fins was investigated by Xu et al. [22], and they found that the performance of staggered arrangement for fins is better than that of parallel arrangement for fins. A modified airfoil fins channel with better thermal-hydraulic performance than NACA0020 airfoil fins channel was proposed by Cui et al. [23]. Zhang et al. [24] conducted experimental studies on PCHE with the modified airfoil fins under the operating conditions of SCO_2 cooler, the results showed that the pressure drop of PCHE with zigzag channel is about 6 times higher than that of PCHE with modified airfoil fins with a roughly equal heat load.

The studies [23,24] indicated that PCHE with modified airfoil fins channel has the better comprehensive performance than PCHEs with zigzag channel and NACA 0020 airfoil fins channel. The experimental and numerical studies about PCHE with modified airfoil fins channel mainly focused on the performance comparison with other compact heat exchangers, and there are little researches about the optimisation of the modified airfoil fins heat exchanger. In this present work, the local thermal-hydraulic characteristics of SCO_2 in the modified airfoil fins channel were investigated under conditions of m = 1.06 g/s to 2.26 g/s, T_{in} = 328.7 K to 388.7 K, q_w = -50 kW/m^2 and -100 kW/m^2. Then two non-uniform distributions of fins were proposed to enhance the overall thermal performance of the modified airfoil fins channel based on the uniformity principle of temperature difference field (TDF) [25]. The thermal-hydraulic performance of channels with different distributions of fins was compared under constant heat flux condition and coupled heat exchange condition. This present work could provide an optimisation strategy for heat exchanger using supercritical fluids as working fluids.

2. Numerical model

2.1. Physical model

As shown in Figure 1, the modified airfoil fins channel in Ref. [24] is selected to establish the physical model. The length, width (W) and height (H) of the model are 270 mm, 4 mm and 0.8 mm. The length (L_s) of inlet and outlet straight section is 15 mm. The length (L) of the main heat exchange region is 240 mm. The length (L_f) of modified airfoil fins is 6 mm. The horizontal pitch (L_{h1}) of modified airfoil fins is 12 mm.

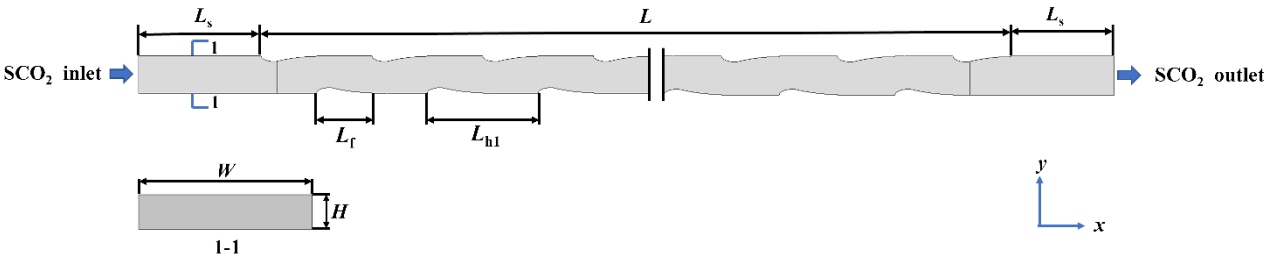

Figure 1. Modified airfoil fins channel with uniform distribution of fins, with L = 240 mm, L_s = 15 mm, L_f = 6 mm, L_{h1} = 12 mm, W = 4 mm, H = 0.8 mm.

2.2. Numerical model

ANSYS CFX 15.0 is employed to conduct the numerical simulation for steady flow. The other assumptions include the effects of axial conduction and the heat exchange with ambient are negligible achieved by ideal insulation. According to Refs. [26,27], the Shear Stress Transport k-ω (SST k-ω) model combines the advantages in the accuracy of k-ε model and the robustness of k-ω model, which could obtain accurate simulation results for supercritical fluids.

Continuity equation:

$$\frac{\partial\left(\rho u_j\right)}{\partial x_j}=0 \tag{1}$$

Momentum equation:

$$\frac{\partial\left(\rho u_i u_j\right)}{\partial x_i}=-\frac{\partial P_i}{\partial x_i}+\frac{\partial}{\partial x_j}\left[\left(\mu+\mu_t\right)\left(\frac{\partial u_i}{\partial x_j}+\frac{\partial u_j}{\partial x_i}-\frac{2}{3}\frac{\partial u_k}{\partial x_k}\right)\right]+\rho g_i \tag{2}$$

Energy equation:

$$\frac{\partial\left(\rho u_j c_p T\right)}{\partial x_j}=\frac{\partial}{\partial x_j}\left(\lambda\frac{\partial T}{\partial x_j}\right)+\Phi \tag{3}$$

where ρ is density, Φ is energy dissipation due to viscosity, g is gravity, c_p represents specific heat at constant pressure, T is temperature, λ represents thermal conductivity, u is velocity, μ represents dynamic viscosity, μ_t represents turbulence viscosity.

Turbulence kinetic energy k:

$$\frac{\partial(\rho k)}{\partial t}+\frac{\partial(\rho k u_i)}{\partial x_i}=\frac{\partial}{\partial x_j}\left(\Gamma_k\frac{\partial k}{\partial x_j}\right)+G_k-Y_k+S_k \tag{4}$$

Specific dissipation rate ω:

$$\frac{\partial(\rho\omega)}{\partial t}+\frac{\partial(\rho\omega u_i)}{\partial x_i}=\frac{\partial}{\partial x_j}\left(\Gamma_\omega\frac{\partial \omega}{\partial x_j}\right)+G_\omega-Y_\omega+S_\omega+D_\omega \tag{5}$$

where Γ_k and Γ_ω are the effective diffusivities of k and ω, G_k is the production of k, G_ω is the generation of ω, Y_k and Y_ω are the dissipations of k and ω caused by turbulence, S_k and S_ω are user-defined source terms, D_ω is cross-diffusion term.

2.3. Boundary conditions

To analyse the local heat transfer coefficient (h) of SCO_2 along the channel with modified airfoil fins under SCO_2 cooler conditions, various constant heat-flux conditions referred from the experiments in Ref. [24] are established and shown in Table 1. The working medium in the fluid region is SCO_2, and the thermophysical properties of SCO_2 referred from the NIST Standard Database [28] are written as a file to input into CFX for simulation. The temperature and mass flux are applied for inlet conditions and pressure is imposed for outlet condition. The left and right surfaces are set as symmetric boundaries. The top, bottom and fins surfaces are set as constant heat-flux boundaries. The dimensionless wall distance (y^+) is set to be less than 1 to assure the accuracy of SST k-ω model. The residual targets of variables for Eqs. (1) to (5) are less than 1×10^{-6} to be considered convergence.

Table 1 Detailed boundary conditions referred from experiments in Ref. [24], minus heat flux denotes working fluid is cooled.

m (g/s)	T_{in} (K)	P_{out} (MPa)	q_w (kW/m^2)
1.06, 1.36, 1.96, 2.26	328.7	8.35	-100

0.96	328.7, 348.7, 368.7, 388.7	8.35	-100
0.96	328.7	8.35	-100, -50

2.4. Grid independence verification and model validation

To complete the grid independence verification, four kinds of grid system are built and Nusselt number (*Nu*) and Fanning friction factor (*f*) of different grids are calculated under conditions of q_w = -100 kW/m^2, T_{in} = 328.7 K and m = 1.06 g/s. In Figure 2, the relative errors of *Nu* and *f* between Grid 3 and Grid 4 are 0.02 % and 0.19 % respectively, indicating simulation results are barely influenced by grid number when grid number is larger than 2.97 million. Considering accuracy and time saving, the Grid 3 with 2.97 million elements is chosen for simulation in this present work.

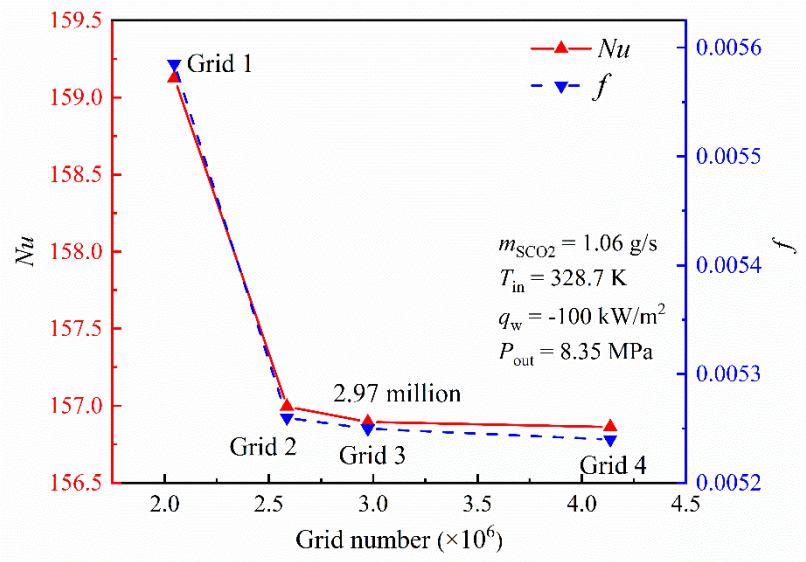

Figure 2. Grid independence verification results for Nusselt number (—▲—) and *f* factor (- -▼- -) at conditions of m = 1.06 g/s, T_{in} = 328.7 K, q_w = -100 kW/m^2, P_{out} = 8.35 MPa under four gird systems.

Coupled model based on the modified airfoil fins heat exchanger in Ref. [24] is established for model validation. Boundary conditions referred the experiment in Ref. [24] are tabulated in Table 2. The model validation results are shown in Table 3. The maximum relative errors of ΔP and Q are 13.82 % and 9.06 % respectively, which means simulation results agree well with experiment results. Therefore, the numerical model is reliable and acceptable in the present work.

Table 2 Detailed boundary conditions for model validation referred the experiment in Ref. [24].

	SCO_2			H_2O		
	m (kg/s)	T_{in} (℃)	P_{out} (MPa)	m (kg/s)	T_{in} (℃)	P_{out} (kPa)
Case 1	0.96×10^{-3}	98.5	8.37	5.56×10^{-3}	16.6	148.3
Case 2	1.27×10^{-3}	100.3	8.53	5.49×10^{-3}	20.6	142.4
Case 3	1.76×10^{-3}	100.8	8.05	5.57×10^{-3}	23.2	144.1

Table 3 Comparison of ΔP and Q between simulation results and experimental data [24].

	Experimental data		Simulation results			
	ΔP (Pa)	Q (kW)	ΔP (Pa)	Q (kW)	ΔP error (%)	Q error (%)
Case 1	900	42.63	780	43.18	13.33	1.29
Case 2	2100	51.69	1990	52.82	5.24	2.19
Case 3	5500	58.61	4740	63.92	13.82	9.06

3. Data reduction

The data processing methods proposed in Refs. [23,29] are adopted in this present work. Quantities of planes are established along the positive direction of x-axis in channel to acquire local thermal-hydraulic parameters such as local Reynolds number (Re_L), local Prandtl number (Pr_L) and local Nusselt number (Nu_L), and overall thermal-hydraulic parameters could be acquired based on local parameters.

The Re_L, Pr_L and Nu_L are obtained as:

$$Re_{\mathrm{L}} = \frac{\rho_{\mathrm{L}} u_{\mathrm{L}} D_{\mathrm{h}}}{\mu_{\mathrm{L}}} \tag{6}$$

$$Pr_{\mathrm{L}} = \frac{\left(\mu c_{\mathrm{p}}\right)_{\mathrm{L}}}{\lambda_{\mathrm{L}}} \tag{7}$$

$$Nu_{\mathrm{L}} = \frac{h_{\mathrm{L}} D_{\mathrm{h}}}{\lambda_{\mathrm{L}}} \tag{8}$$

where D_{h} represents hydraulic diameter.

The local h is expressed as:

$$h_{\mathrm{L}} = \frac{q_{\mathrm{w,L}}}{T_{\mathrm{w,L}} - T_{\mathrm{b,L}}} \tag{9}$$

where q represents heat flux, subscripts L, w and b represent local, wall and bulk.

The calculation methods of D_{h1} and D_{h2} for channel with uniform and dense distributions of fins are presented as follows [30,31]:

$$D_{\mathrm{h1}} = \frac{4V_{\mathrm{u}}}{S_{\mathrm{u}}} \tag{10}$$

$$V_{\mathrm{u}} = L_{\mathrm{h1}} WH - V_{\mathrm{f}} \tag{11}$$

$$S_{\mathrm{u}} = 2L_{\mathrm{h1}} W + S_{\mathrm{f,side}} - 2S_{\mathrm{f,top}} \tag{12}$$

$$D_{\mathrm{h2}} = \frac{4(L_{\mathrm{h3}} WH - 2V_{\mathrm{f}})}{(2L_{\mathrm{h3}} W + 2S_{\mathrm{f,side}} - 4S_{\mathrm{f,top}})} \tag{13}$$

where V_{u} is the volume of periodic unit shown in Figure 3, S_{u} is the surface area of periodic unit, $S_{\mathrm{f,side}}$ and $S_{\mathrm{f,top}}$ are the area of side surface and top surface for the modified airfoil fins.

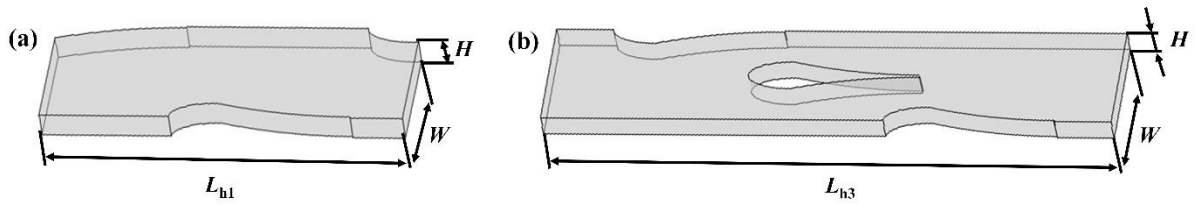

Figure 3. Periodic units to define the hydraulic diameter of channel with (a) uniform and (b) dense distributions of fins, with W = 4 mm, H = 0.8 mm, L_{h1} = 12 mm, L_{h3} = 20 mm.

The local heat transfer factor (j), friction factor (f) and comprehensive performance criterion (CPC) [29] are obtained as:

$$j_{\mathrm{L}} = \frac{Nu_{\mathrm{L}}}{Re_{\mathrm{L}} Pr_{\mathrm{L}}^{1/3}} \tag{14}$$

$$f_L = \frac{\Delta P_L}{2u_L^2 \rho_L} \cdot \frac{D_h}{\Delta l} \tag{15}$$

$$CPC = \frac{j/j_0}{\left(f/f_0\right)^{1/3}} \tag{16}$$

where the subscript 0 represents the parameter of channel with uniform distribution of fins.

4. Results and discussion

In this section, the local h of SCO_2 in the modified airfoil fins channel is investigated firstly under conditions of m = 1.06 g/s to 2.26 g/s, T_{in} = 328.7 K to 388.7 K, q_w = -50 kW/m^2 and -100 kW/m^2. Then, two non-uniform distributions of fins are proposed to enhance the overall thermal performance by improving the distribution uniformity of ΔT along the channel. The overall h and ΔP of channels with different distributions of fins are compared and the heat transfer mechanism is analysed. Finally, the effects of two non-uniform distributions of fins on the thermal-hydraulic performance of the coupled heat transfer model are evaluated.

4.1. Local heat transfer characteristics

In this work, the T_{in} of SCO_2 is from 328.7 K to 388.7 K and the T_b of SCO_2 would be cooled to be around T_{pc} (about 309.7 K at 8.35 MPa), leading to the dramatic changes of local heat transfer characteristic of SCO_2 along the positive direction of x-axis in channel. In Ref. [32], T_b/T_{pc} of SCO_2 was used to evaluate the overall thermal performance of SCO_2 in PCHE. Analogy to this evaluation method, T_b/T_{pc} is adopted to delineate the region near pseudocritical point ($0.99 < T_b/T_{pc} < 1.02$). The changes of thermophysical properties for SCO_2 is dramatic in the region near pseudocritical point ($0.99 < T_b/T_{pc} < 1.02$).

The variations of local T_b and h along the x-axis positive direction under conditions of m = 1.06 g/s to 2.26 g/s, T_{in} = 328.7 K, q_w = -100 kW/m^2 and P_{out} = 8.35 MPa are presented in Figure 4. The region near pseudocritical point ($0.99 < T_b/T_{pc} < 1.02$) is mainly located in the region of x from 0 mm to 120 mm at m= 1.06 g/s and moves to the region of x from 120 mm to 240 mm when m increases to 2.26 g/s, which affect the distribution of local h along the x-axis positive direction. As seen in Figure 4(b), h_{peak} appears at x = 66 mm at m = 1.06 g/s and moves to the location at x = 174 mm when m increases to 2.26 g/s. In Figure 5, the region near pseudocritical point ($0.99 < T_b/T_{pc} < 1.02$) from the region of x from 0 mm to 120 mm moves to the region of x from 120 mm to 240 mm and the position of h_{peak} from x = 54 mm moves to x = 162 mm when T_{in} changes from 328.7 K to 388.7 K. In Figure 6, the region near pseudocritical point ($0.99 < T_b/T_{pc} < 1.02$) from the region

of x from 0 mm to 120 mm moves to the region of x from 120 mm to 240 mm and the position of h_{peak} from x = 54 mm moves to x = 150 mm when q_w changes from -100 kW/m^2 to -50 kW/m^2. The region near pseudocritical point ($0.99 < T_b/T_{pc} < 1.02$) in channel is variable under different cooling conditions, leading to the uneven distribution of local h along the modified airfoil fins channel.

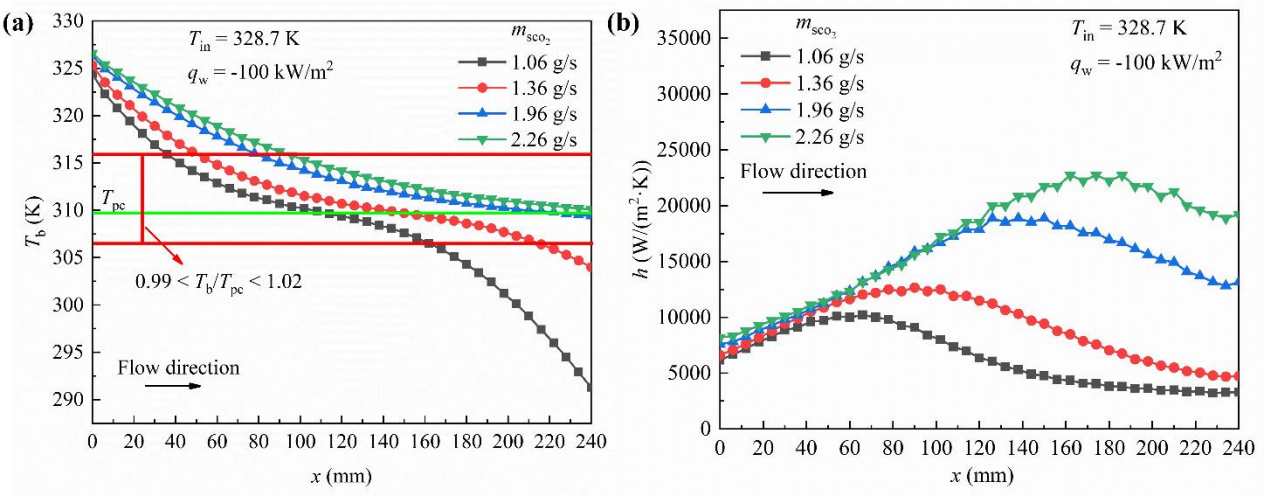

Figure 4. Distributions of local (a) T_b and (b) h along the x-axis positive direction in channel with evenly distributed fins under conditions of q_w = -100 kW/m^2, T_{in} = 328.7 K, P_{out} = 8.35 MPa, m = 1.06 g/s (—■—), m = 1.36 g/s (—●—), m = 1.96 g/s (—▲—), m = 2.26 g/s (—▼—).

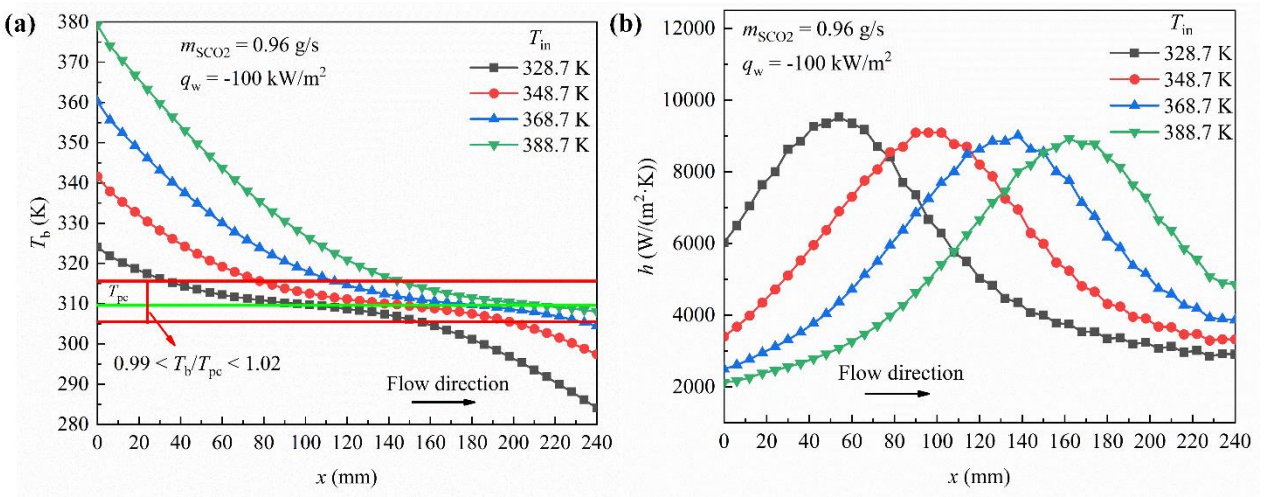

Figure 5. Distributions of local (a) T_b and (b) h along the x-axis positive direction in channel with evenly distributed fins under conditions of q_w = -100 kW/m^2, m = 0.96 g/s, P_{out} = 8.35 MPa, T_{in} = 328.7 K (—■—), T_{in} = 348.7 K (—●—), T_{in} = 368.7 K (—▲—), T_{in} = 388.7 K (—▼—).

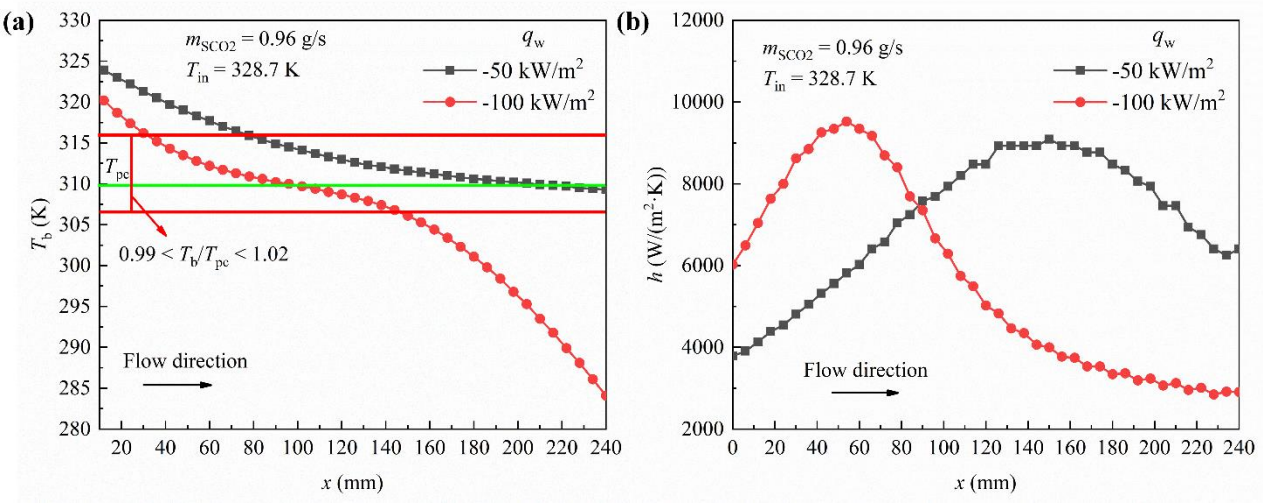

Figure 6. Distributions of local (a) T_b and (b) h along the x-axis positive direction in channel with evenly distributed fins under conditions of m = 0.96 g/s, T_{in} = 328.7 K, P_{out} = 8.35 MPa, q_w = -50 kW/m^2 (—■—), q_w = -100 kW/m^2 (—●—).

4.2. Two non-uniform distributions of airfoil fins

It could be concluded from Eq. (9) that the smaller local ΔT represents the larger local h under constant wall heat-flux condition. According to the uniformity principle of TDF [25], the redistribution of heat exchange area is an effective approach to improve the uniformity of TDF in heat exchanger to enhance thermal performance. In this work, the local heat exchange area could be redistributed by changing the positions of fins when the total number of fins and total heat exchange area are constant. Thus, two channels with non-uniform distributions of fins are proposed, including the channel with front-dense and rear-sparse (FDRS) distribution of fins and the channel with front-sparse and rear-dense (FSRD) distribution of fins.

The channels with FDRS and FSRD distributions of fins are presented in Figure 7. The total length of two channels and the total number of fins are the same as the channel shown in Figure 1. The horizontal pitches (L_{h3} and L_{h4}) of fins in the region with dense distribution of fins are 20 mm and 4 mm, respectively. The horizontal pitch (L_{h2}) of fins in the region with sparse distribution of fins is 15 mm.

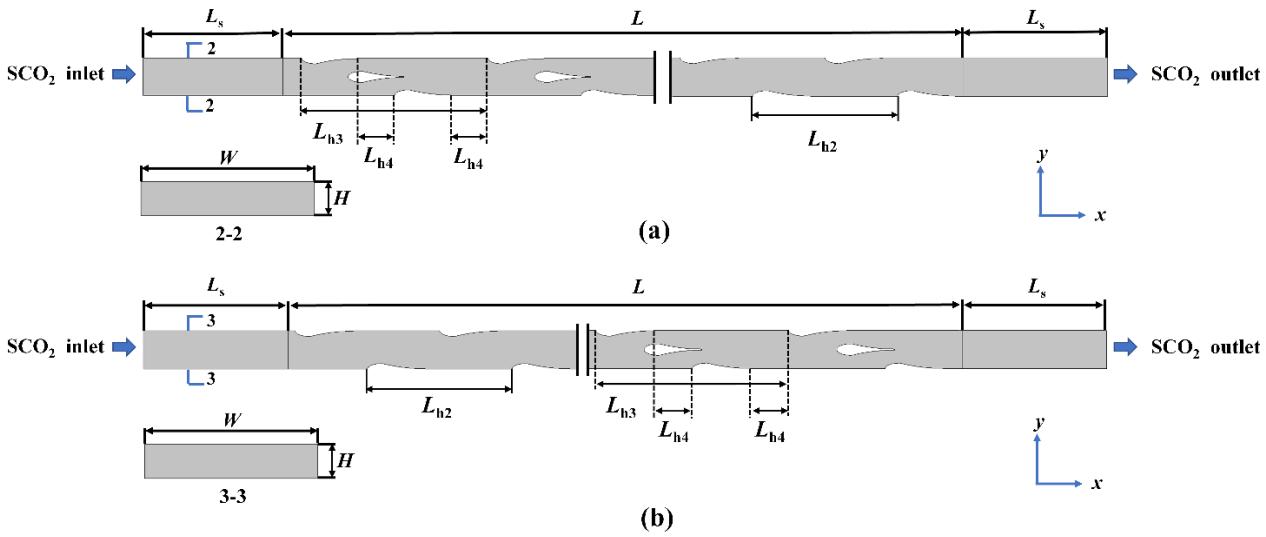

Figure 7. Channels with (a) front-dense and rear-sparse and (b) front-sparse and rear-dense distributions of fins, with L = 240 mm, L_s = 15 mm, L_f = 6 mm, L_{h2} = 15 mm, L_{h3} = 20 mm, L_{h4} = 4 mm, W = 4 mm, H = 0.8 mm.

To investigate the effect of FDRS and FSRD distributions of fins on the thermal-hydraulic performance, the overall h and ΔP of uniform, FDRS and FSRD distributions are compared under the boundary conditions listed in Table 1. As seen in Figure 8(a), the overall h of FDRS and FSRD distributions are 5.1 % to 13 % higher than that of uniform distribution under conditions of m = 1.06 g/s to 2.26 g/s, T_{in} = 328.7 K and q_w = -100 kW/m^2. It could be found from Figures 8(a) and 4 that the region near pseudocritical point ($0.99 < T_b/T_{pc} < 1.02$) with higher local h is mainly concentrated in the region of x from 0 mm to 120 mm at m = 1.06 g/s to 1.36 g/s, and the overall h of FDRS distribution is 2.9 % to 5.5 % higher than that of FSRD distribution. However, the region near pseudocritical point ($0.99 < T_b/T_{pc} < 1.02$) with higher local h is mainly concentrated in the region of x from 120 mm to 240 mm at m = 1.96 g/s to 2.26 g/s, and the overall h of FSRD distribution is 2.1 % to 3.3 % higher than that of FDRS distribution.

In Figures 9(a) and 5, the overall h of FDRS and FSRD distributions are 8.4 % to 12.5 % higher than that of uniform distribution under conditions of m = 0.96 g/s, q_w = -100 kW/m^2 and T_{in} = 328.7 K to 388.7 K. At T_{in} = 328.7 K to 348.7 K, the region near pseudocritical point ($0.99 < T_b/T_{pc} < 1.02$) with higher local h is mainly concentrated in the region of x from 0 mm to 120 mm and the overall h of FDRS distribution is 0.5 % to 2.8 % higher than that of FSRD distribution. At T_{in} = 368.7 K to 388.7 K, the region near pseudocritical point ($0.99 < T_b/T_{pc} < 1.02$) with higher local h is mainly concentrated in the region of x from 120 mm to 240 mm and the overall h of FSRD distribution is 1.5 % to 3.3 % higher than that of FDRS distribution.

In Figures 10(a) and 6, the overall h of FDRS and FSRD distributions are 8.4 % to 13.3 % higher than that of uniform distribution under conditions of m = 0.96 g/s, T_{in} = 328.7 K, q_w=-50 kW/m^2 and -100 kW/m^2. At q_w = -100 kW/m^2, the region near pseudocritical point (0.99 < T_b/T_{pc} < 1.02) with higher local h is mainly concentrated in the region of x from 0 mm to 120 mm and the overall h of FDRS distribution is 2.8 % higher than that of FSRD distribution. At q_w = -50 kW/m^2, the region near pseudocritical point (0.99 < T_b/T_{pc} < 1.02) with higher local h is mainly concentrated in the region of x from 120 mm to 240 mm and the overall h of FSRD distribution is 2.4 % higher than that of FDRS distribution.

From the above comparisons of overall h between FDRS and FSRD distributions, it could be concluded that local dense distribution of fins matches with the region near pseudocritical point (0.99 < T_b/T_{pc} < 1.02) where the peak of h appears, leading to the better overall thermal performance. In addition, it could be seen in Figures 8(b), 9(b) and 10(b) that the overall ΔP of FDRS and FSRD distributions are 1.5 % to 8.8 % higher than that of uniform distribution. The overall ΔP of FDRS distribution is 3.3 % to 7 % higher than that of FSRD distribution. Thus, the comparison of comprehensive thermal-hydraulic performance among the three distributions of fins should be further considered.

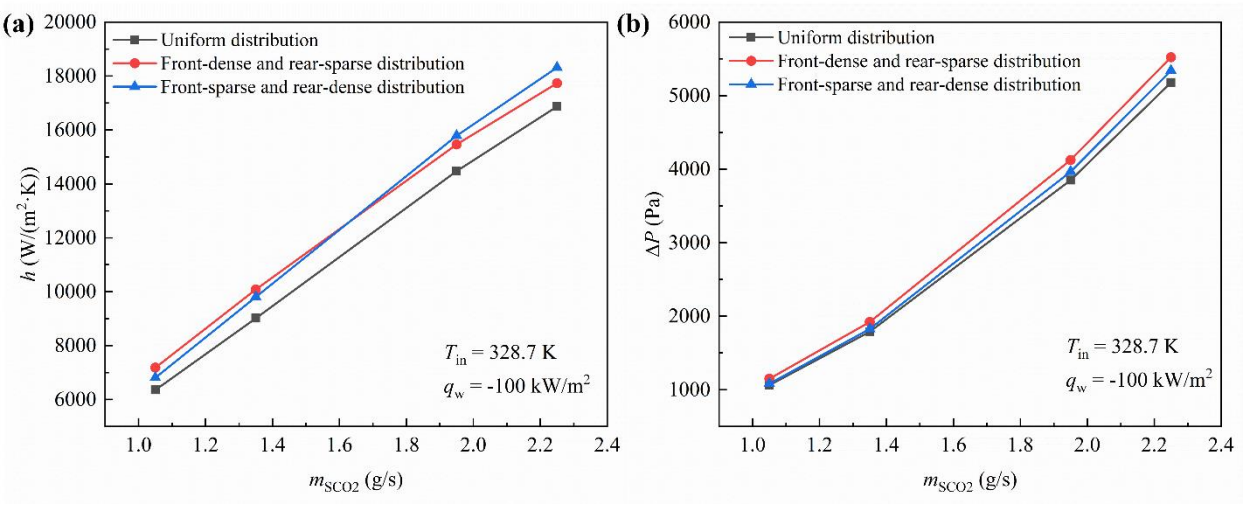

Figure 8. Comparisons of (a) h and (b) ΔP among uniform distribution (—■—), FDRS distribution (—●—), FSRD distribution (—▲—) under conditions of m = 1.06 g/s to 2.26 g/s, T_{in} = 328.7 K, q_w = -100 kW/m^2, P_{out} = 8.35 MPa.

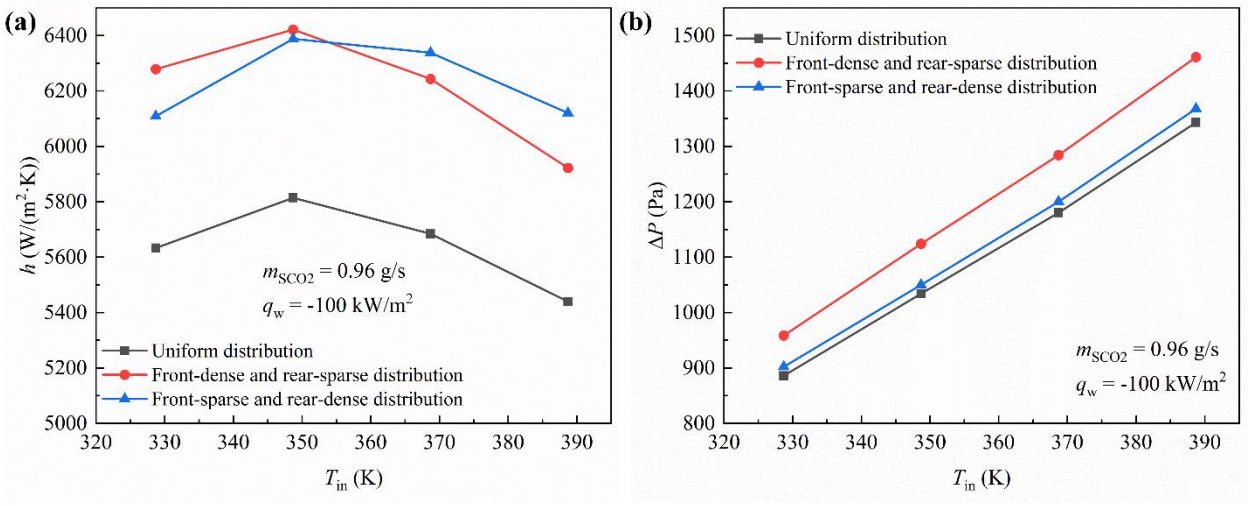

Figure 9. Comparisons of (a) h and (b) ΔP among uniform distribution (—■—), FDRS distribution (—●—), FSRD distribution (—▲—) under conditions of m = 0.96 g/s, T_{in} = 328.7 K to 388.7 K, q_w = -100 kW/m^2, P_{out} = 8.35 MPa.

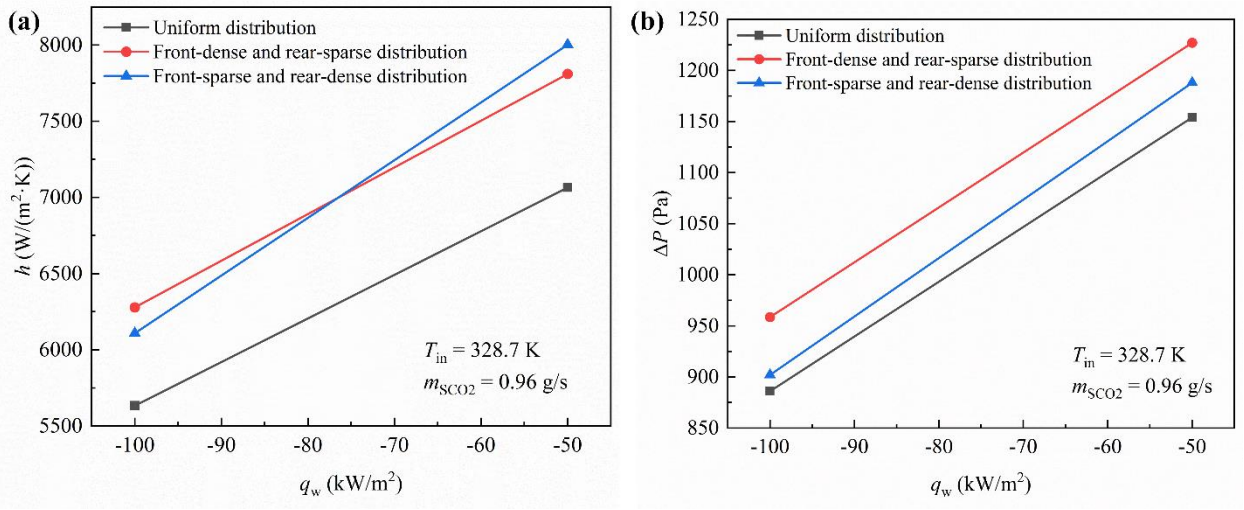

Figure 10. Comparisons of (a) h and (b) ΔP among uniform distribution (—■—), FDRS distribution (—●—), FSRD distribution (—▲—) under conditions of m = 0.96 g/s, T_{in} = 328.7 K, q_w = -100 kW/m^2 and -50 kW/m^2, P_{out} = 8.35 MPa.

4.3. Analyses of heat transfer and flow mechanism

The field synergy principle proposed by Guo et al. [33] could reveal the mechanism of heat transfer enhancement components very well [34-36] and is employed here.

$$Nu = RePr\iiint_V \left(\overline{\boldsymbol{U}}\cdot\nabla\overline{\boldsymbol{T}}\right)d\overline{V} \tag{17}$$

$$\overline{\boldsymbol{U}} \cdot \nabla \overline{\boldsymbol{T}} = \left|\overline{\boldsymbol{U}}\right| \cdot \left|\nabla \overline{\boldsymbol{T}}\right| \cos\alpha \tag{18}$$

where $\nabla \overline{\boldsymbol{T}}$ is dimensionless temperature gradient, $\overline{\boldsymbol{U}}$ is dimensionless velocity, α is the synergy angle between $\overline{\boldsymbol{U}}$ and $\nabla \overline{\boldsymbol{T}}$.

It could be found from Eqs. (17) and (18) that the smaller α indicates the better synergy between $\overline{\boldsymbol{U}}$ and $\nabla \overline{\boldsymbol{T}}$ in channel, corresponding to the better thermal performance. As seen in Figure 11, the α of FDRS and FSRD distributions are 3.3 % to 4.6 % smaller than that of uniform distribution under conditions of m = 1.06 g/s to 2.26 g/s, T_{in} = 328.7 K and q_w = -100 kW/m^2, indicating FDRS and FSRD distributions of fins could improve the synergy between $\overline{\boldsymbol{U}}$ and $\nabla \overline{\boldsymbol{T}}$. The effect of FDRS and FSRD distributions on the synergy improvement between $\overline{\boldsymbol{U}}$ and $\nabla \overline{\boldsymbol{T}}$ is visualised in Figure 12. Moreover, the α of FDRS distribution is 0.49 % to 0.6 % smaller than that of FSRD distribution at m = 1.06 g/s to 1.36 g/s, which means the overall thermal performance of FDRS distribution is better than that of FSRD distribution. The α of FSRD distribution is 0.65 % to 0.73 % smaller than that of FDRS distribution at m = 1.96 g/s to 2.26 g/s, which indicates the overall thermal performance of FSRD distribution is better than that of FDRS distribution.

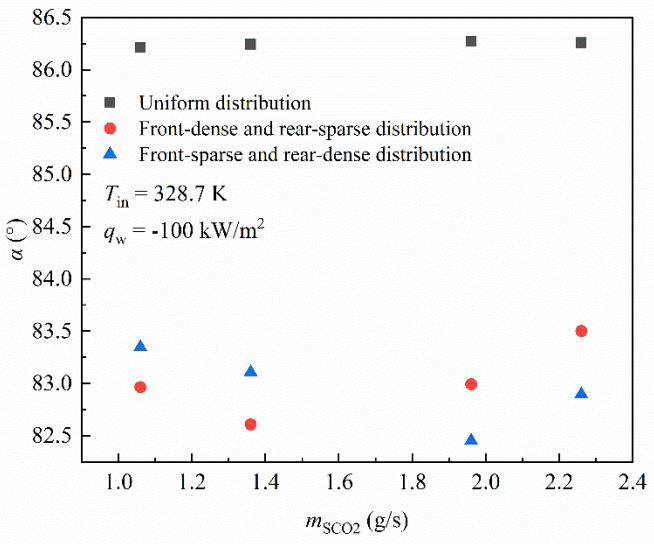

Figure 11. Comparison of field synergy angle α among uniform distribution (■), FDRS distribution (●), FSRD distribution (▲) under conditions of m = 1.06 g/s to 2.26 g/s, T_{in} = 328.7 K, q_w = -100 kW/m^2, P_{out} = 8.35 MPa.

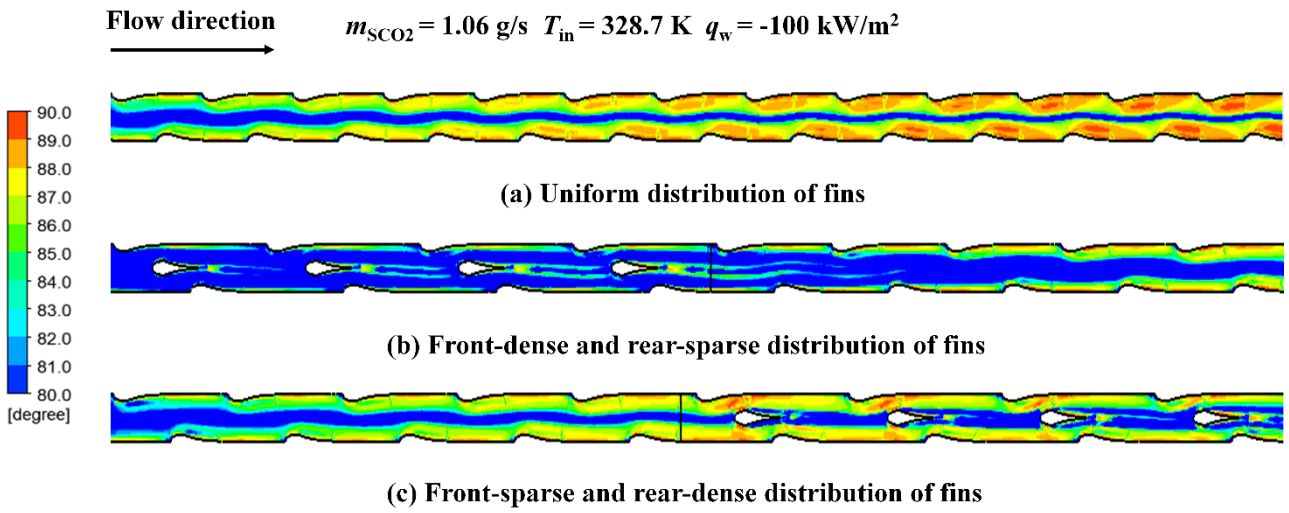

Figure 12. Distribution of field synergy angle α in channels with (a) uniform, (b) FDRS, (c) FSRD distributions of fins under conditions of m = 1.06 g/s, T_{in} = 328.7 K, q_w = -100 kW/m^2, P_{out} = 8.35 MPa.

The field synergy principle was extended to the analysis of flow resistance by Liu et al. [37], the dimensionless ΔP is given as [37]:

$$\Delta \overline{P} = \frac{\Delta P}{\rho u^2} = \frac{0.646 l / L}{\sqrt{Re}\sqrt{l/H}} + \frac{3\left(1 - l / L\right)}{Re} + \iiint_V \left(\overline{\boldsymbol{U}} \cdot \nabla \overline{\boldsymbol{U}}\right) d\overline{\boldsymbol{V}} \tag{19}$$

$$\overline{\boldsymbol{U}} \cdot \nabla \overline{\boldsymbol{U}} = \left|\overline{\boldsymbol{U}}\right| \cdot \left|\nabla \overline{\boldsymbol{U}}\right| \cos\beta \tag{20}$$

where $\nabla \overline{\boldsymbol{U}}$ is dimensionless velocity gradient, β is the synergy angle between $\overline{\boldsymbol{U}}$ and $\nabla \overline{\boldsymbol{U}}$.

From Eqs. (19) and (20), it could be found that the larger β indicates the smaller $\Delta \overline{P}$ and better hydraulic performance. As shown in Figure 13, the β of uniform distribution is 5 % to 6.8 % larger than that of FDRS and FSRD distributions at m = 1.06 g/s to 2.26 g/s, which reveals the hydraulic performance deterioration caused by local dense distributions of fins cannot be ignored. The β of FSRD distribution is 0.5 % to 1 % larger than that of FDRS distribution at m = 1.06 g/s to 2.26 g/s, indicating the hydraulic performance of FDRS distribution is worse than that of FSRD distribution.

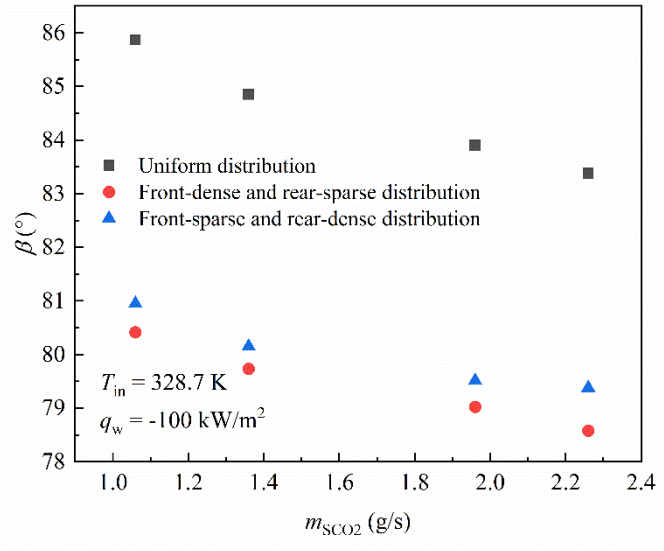

Figure 13. Comparison of field synergy angle β among uniform distribution (■), FDRS distribution (●), FSRD distribution (▲) under conditions of m = 1.06 g/s to 2.26 g/s, T_{in} = 328.7 K, q_w = -100 kW/m^2, P_{out} = 8.35 MPa.

Based on the second law of thermodynamics, the irreversible losses of heat transfer and flow resistance are employed to further evaluate the thermal performance enhancement and hydraulic performance deterioration. The entropy generation proposed by Bejan et al. [38] is widely used in the analysis of irreversible losses, and the local entropy generation related to heat transfer and flow resistance could be defined as [38]:

$$\dot{S}_{g,\Delta T} = \frac{\lambda}{T^2}\left[\left(\frac{\partial T}{\partial x}\right)^2 + \left(\frac{\partial T}{\partial y}\right)^2 + \left(\frac{\partial T}{\partial z}\right)^2\right] \tag{21}$$

$$\dot{S}_{g,\Delta P} = \frac{\mu}{T}\left\{\begin{array}{l} 2\left[\left(\frac{\partial u_x}{\partial x}\right)^2 + \left(\frac{\partial u_y}{\partial y}\right)^2 + \left(\frac{\partial u_z}{\partial z}\right)^2\right] \\ + \left(\frac{\partial u_x}{\partial y} + \frac{\partial u_y}{\partial x}\right)^2 + \left(\frac{\partial u_x}{\partial z} + \frac{\partial u_z}{\partial x}\right)^2 + \left(\frac{\partial u_y}{\partial z} + \frac{\partial u_z}{\partial y}\right)^2 \end{array}\right\} \tag{22}$$

To facilitate the comparison of entropy generation for different distributions of fins, the dimensionless entropy generation number defined by Hesselgreaves et al. [39] is used to evaluate the irreversible losses of different distributions of fins, which could be expressed as:

$$N_{s,\Delta T} = \frac{\iiint_V \dot{S}_{g,\Delta T}\mathrm{d}V}{\dot{Q}/T_{in}} \tag{1}$$

$$N_{s,\Delta P} = \frac{\iiint_V \dot{S}_{g,\Delta P}\mathrm{d}V}{\dot{Q}/T_{in}} \tag{2}$$

where $\dot{Q}$ is heat transfer rate.

As shown in Figure 14, the $N_{s,\Delta T}$ of FDRS and FSRD distributions are 2 % to 9 % smaller than that of uniform distribution at m = 1.06 g/s to 2.26 g/s, which means the thermal performance of FDRS and FSRD distributions is better than that of uniform distribution. The $N_{s,\Delta P}$ of uniform distribution is 55 % to 74 % smaller than that of FDRS distribution and is 12 % to 30 % smaller than that in channel with FSRD distribution of fins, which indicates the hydraulic performance of FDRS distribution is the worst among uniform, FDRS and FSRD distributions.

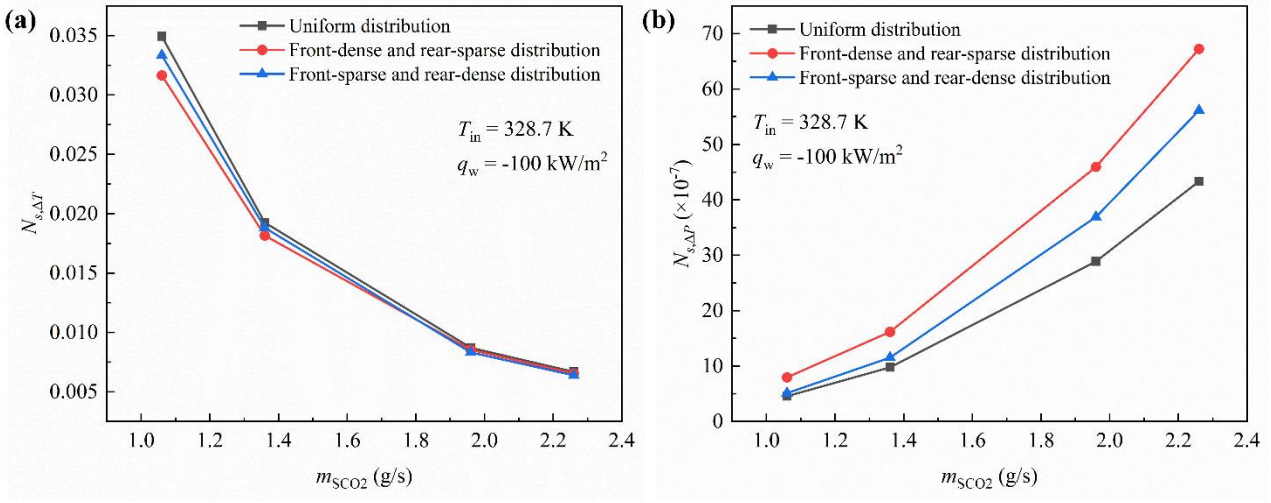

Figure 14. Comparisons of (a) $N_{s,\Delta T}$ and (b) $N_{s,\Delta P}$ among uniform distribution (—■—), FDRS distribution (—●—), FSRD distribution (—▲—) under conditions of m = 1.06 g/s to 2.26 g/s, T_{in} = 328.7 K, q_w = -100 kW/m^2, P_{out} = 8.35 MPa.

4.4. Performance comparisons of different distributions of fins

In section 4.2, the effects of FDRS and FSRD distributions of fins on the thermal-hydraulic performance of modified airfoil fins channel under constant heat-flux conditions are analysed in detail. However, there is a complex coupled heat transfer process between SCO_2 and H_2O in real SCO_2 cooler, and the wall heat-flux is variable. It is essential to analyse the effects of FDRS and FSRD distributions on the thermal-hydraulic performance in the coupled heat transfer model.

In Figure 15, uniform, FDRS and FSRD distributions of fins are arranged in the hot-side channel of three coupled models respectively, and uniform distribution of fins is arranged in the cold-side channel of three

coupled models. The length (L_2), width (W_2) and height (H_2) of three models are 270 mm, 4 mm and 3.6 mm. The wall thickness (t_w) between hot-side channel and cold-side channel is 1 mm.

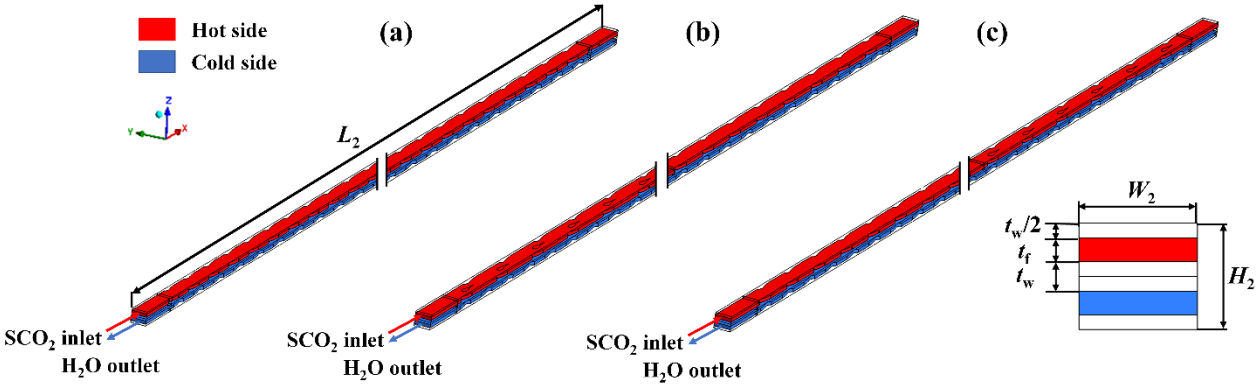

Figure 15. Three coupled models with (a) uniform, (b) FDRS and (c) FSRD distributions of fins in hot-side channel, with L_2 = 270 mm, W_2 = 4 mm, H_2 = 3.6 mm, t_w = 1 mm.

For coupled heat transfer model, the working mediums in fluid domain are H_2O and SCO_2, and the material in solid domain is 316L stainless steel. The top and bottom surfaces in coupled model are periodic, and the left and right surfaces are symmetric. The interfaces between fluid and solid domains are assigned as smooth and non-slip walls, and the other surfaces are adiabatic. Several conditions are set in Table 4 to explore the influence of two non-uniform distributions of fins on the thermal-hydraulic performance of SCO_2 in the coupled models.

Table 4 Detailed boundary conditions of coupled heat exchange model, SCO_2 and H_2O are working mediums in hot and cold sides.

	Hot-side (SCO_2)			Cold-side (H_2O)		
	m (kg/s)	T_{in} (°C)	P_{out} (MPa)	m (kg/s)	T_{in} (°C)	P_{out} (kPa)
Case1	0.96×10^{-3}	70.6	8.35	5.47×10^{-3}	16.4	147
Case2	1.86×10^{-3}	70.6	8.35	5.47×10^{-3}	16.4	147
Case3	0.96×10^{-3}	154.8	8.35	5.47×10^{-3}	16.4	147

Case4	0.96	70.6	8.35	1.47	16.4	147

The thermal-hydraulic performance for hot-side channel in three models is evaluated by *j* factor, *f* factor and *CPC*. As shown in Figure 16(a), the *j* factor of channels with FDRS and FSRD distributions are 21 % to 30 % higher than that of channel with uniform distribution under Cases 1 to 4. The *j* factor of channel with FDRS distribution of fins is 2 % higher than that of channel with FSRD distribution under Case 1, and the *j* factor of channel with FSRD distribution is 2.4 % to 2.8 % higher than that of channel with FDRS distribution under Cases 2 to 4. Combined with Figure 17, it could be seen that the region near pseudocritical point ($0.99 < T_b/T_{pc} < 1.02$) with higher local *h* is mainly concentrated in the region of *x* from 0 mm to 120 mm under Case 1 and is mainly concentrated in the region of *x* from 120 mm to 240 mm under Cases 2 to 4. Thus, the match of local dense distributions of fins with the region where the peak of *h* appears could obtain better overall thermal performance. In Figure 16(b), the *f* factor of channel with FDRS distribution of fins is 7.5 % to 17 % higher than that of channel with uniform distribution of fins and is 3.9 % to 14.3 % higher than that of channel with FSRD distribution of fins under Cases 1 to 4, indicating the hydraulic performance of channel with FDRS distribution of fins is the worst.

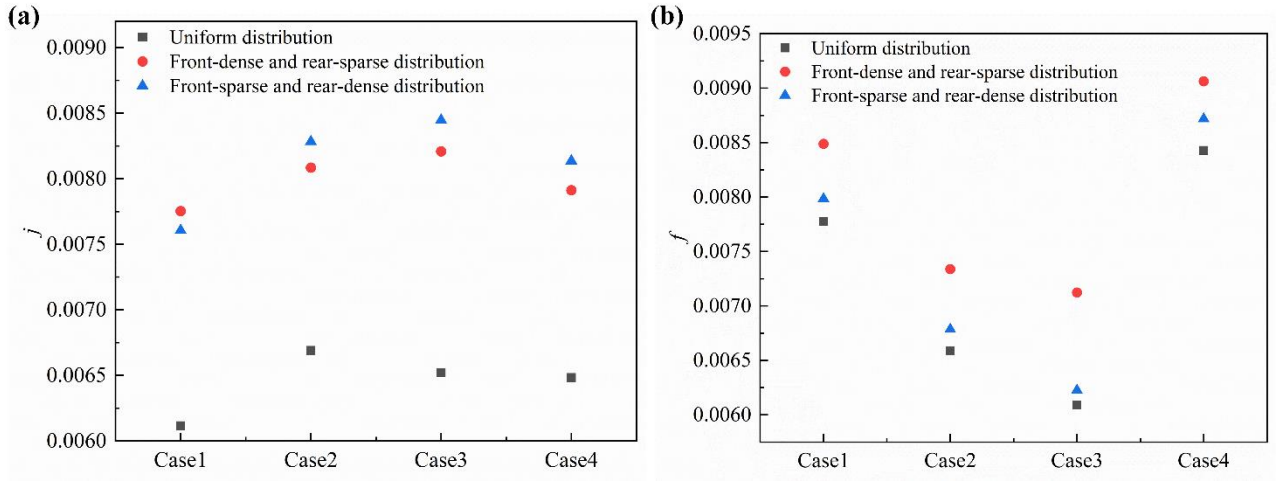

Figure 16. Comparisons of (a) *j* factor and (b) *f* factor among hot-side channles with uniform distribution of fins (■), FDRS distribution of fins (●), FSRD distribution of fins (▲) under Cases 1 to 4.

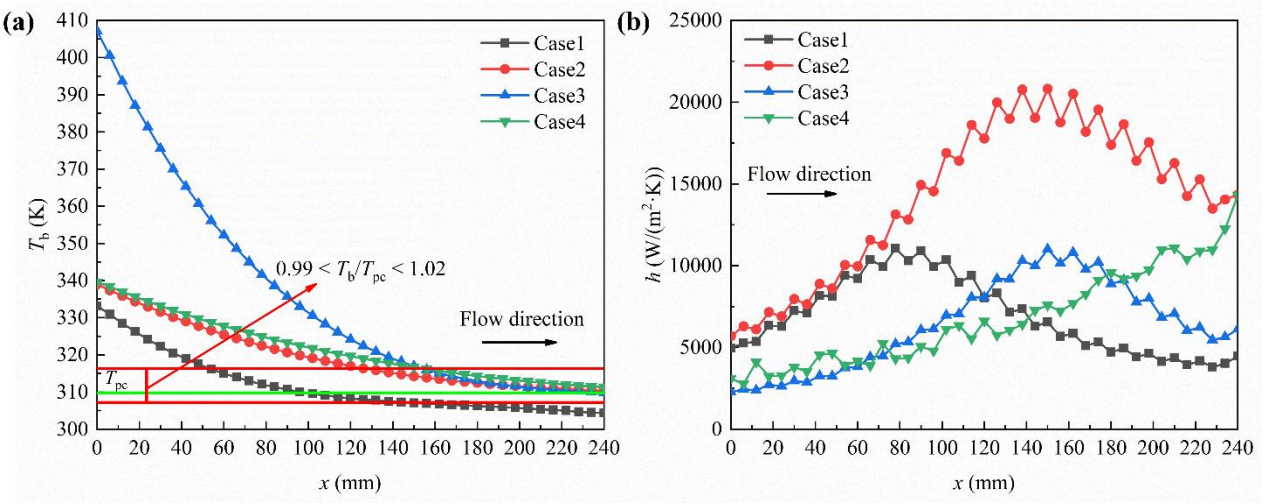

Figure 17. Distributions of local (a) T_b and (b) h along the x-axis positive direction in hot-side channel with uniform distribution of fins under Case 1 (—■—), Case 2 (—●—), Case 3 (—▲—), Case 4 (—▼—).

To evaluate the comprehensive performance of channels with uniform, FDRS and FSRD distributions of fins, the comparison of *CPC* among the three channels under Cases 1 to 4 is presented in Figure 18. The *CPC* of channel with FSRD distribution of fins is 23 % to 29 % higher than that of channel with uniform distribution of fins and is 2 % to 7.6 % higher than that of channel with FDRS distribution of fins under Cases 1 to 4. Therefore, the comprehensive performance of channel with FSRD distribution of fins is the best among channels with uniform, FDRS and FSRD distributions of fins, and the FSRD distribution of fins is the optimum scheme for the distribution optimisation of fins in the modified airfoil fins channel.

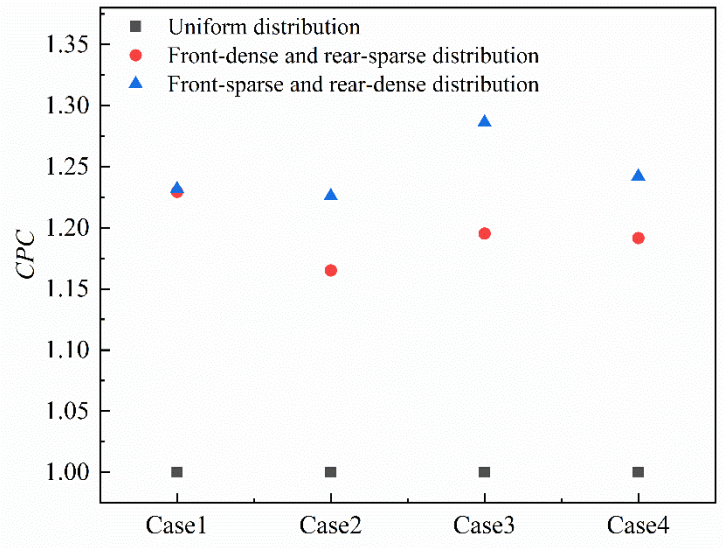

Figure 18. Comparison of *CPC* among hot-side channles with uniform distribution of fins (■), FDRS distribution of fins (●), FSRD distribution of fins (▲) under Cases 1 to 4.

5. Conclusions

The local thermal characteristics of SCO_2 in the modified airfoil fins channel are numerically investigated under conditions of m = 1.06 g/s to 2.26 g/s, T_{in} = 328.7 K to 388.7 K, q_w = -50 kW/m^2 and -100 kW/m^2. Two non-uniform distributions of modified airfoil fins are proposed to enhance the overall thermal performance, and the thermal-hydraulic performance of channels with uniform, front-dense and rear-sparse (FDRS) and front-sparse and rear-dense (FSRD) distributions of modified airfoil fins are compared. The conclusions summarized in this present work are listed as follows:

(1) The dramatic changes of thermophysical properties of SCO_2 lead to the uneven distributions of local h and ΔT along channel especially in the region near pseudocritical point ($0.99 < T_b/T_{pc} < 1.02$). Based on the uniformity principle of TDF, two non-uniform distributions of fins including the FDRS and FSRD distributions of fins are proposed. The overall distribution uniformity of ΔT in channel could be improved by FDRS and FSRD distributions of fins to strengthen the overall thermal performance.

(2) Under conditions of m = 1.06 g/s to 2.26 g/s, T_{in} = 328.7 K to 388.7 K, q_w = -50 kW/m^2 and -100 kW/m^2, the overall h of channels with FDRS and FSRD distributions of fins are 5.1 % to 13.3 % higher than that of channel with uniform distribution of fins, so the overall thermal performance could be improved by FDRS and FSRD distributions of fins. The overall ΔP of channels with FDRS and FSRD distributions of fins are 1.5% to 8.8 % higher than that of channel with uniform distribution of fins, indicating FDRS and FSRD distributions of fins increase the flow resistance. The differences of thermal-hydraulic performance among channels with uniform, FDRS and FSRD distributions of fins could be explained by field synergy principle.

(3) The comparison of thermal performance between FDRS and FSRD distribution of fins indicates that the match of local dense distribution of fins with the region near pseudocritical point ($0.99 < T_b/T_{pc} < 1.02$) where the peak of h appears, could obtain better overall thermal performance in the modified airfoil fins heat exchanger using as SCO_2 cooler.

(4) Under the coupled heat transfer process between SCO_2 and H_2O, the *CPC* of channel with FSRD distribution of fins is 23 % to 29 % higher than that of channel with uniform distribution of fins and is 2 % to 7.6 % higher than that of channel with FDRS distribution of fins. The FSRD distribution of fins is the optimum scheme among the three distributions of fins for the distribution optimisation of fins in the channel.

Acknowledgements

This project has received funding from the National Energy Group Major Pilot Project-China (GJNY2030XDXM-19-10) and the European Union's Horizon 2020 research and innovation programme under the Marie Skłodowska-Curie grant agreement No [882628].

Nomenclature

A	heat exchange area (m^2)
c_p	specific heat at constant pressure [J/(kg·K)]
CPC	comprehensive performance criteria
D_h	hydraulic diameter (m)
f	Fanning friction factor
FDRS	front-dense and rear-sparse
FSRD	front-sparse and rear-dense
g	gravity (m/s^2)
h	heat transfer coefficient [$W/(m^2 \cdot K)$]
H	height of the channels (m)
H_2	height of the models (m)
j	Colburn-j factor
l	inlet length (m)
L	length of main heat exchange area (m)
L_2	length of model (m)
L_f	length of fins (m)
L_h	horizontal pitch of fins (m)
L_s	length of inlet and outlet straight section (m)
m	mass flow rate (kg/s)
Nu	Nusselt number
N_s	dimensionless entropy generation number
P	pressure (MPa)
Pr	Prandtl number

q_w wall heat flux (kW/m^2)

Q heat transfer rate (kW)

Re Reynolds number

S surface area (m^2)

$\dot{S}_g$ entropy generation rate per unit volume [W/(m^3·K)]

T temperature (K)

TDF temperature difference field

$\nabla\overline{\boldsymbol{T}}$ dimensionless temperature gradient

u velocity (m/s)

$\overline{\boldsymbol{U}}$ dimensionless velocity

$\nabla\overline{\boldsymbol{U}}$ dimensionless velocity gradient

V volume (m^3)

W width of channels (m)

W_2 width of models (m)

x length in positive x-axis direction (m)

Greek symbols

α field synergy angle between temperature gradient and velocity fields (°)

β filed synergy angle between pressure and pressure gradient fields (°)

ΔP pressure drop (Pa)

λ thermal conductivity [W/(m·K)]

μ dynamic viscosity (Pa·s)

μ_t turbulence viscosity (Pa·s)

ρ density [kg/m^3]

Φ energy dissipation caused by viscosity [W/m^2]

Subscripts

b bulk

f fins

L local cross-section

s solid

w wall

References

[1] Y.L. Moullec, Conceptual study of a high efficiency coal-fired power plant with CO_2 capture using a supercritical CO_2 Brayton cycle, Energy 49 (2013) 32-46. https://doi.org/10.1016/j.energy.2012.10.022.

[2] C.S. Turchi, Z. Ma, T.W. Neises, M.J. Wagner, Thermodynamic Study of Advanced Supercritical Carbon Dioxide Power Cycles for Concentrating Solar Power Systems, J. Sol. Energy Eng. 135 (4) (2013) 041007. https://doi.org/10.1115/1.4024030.

[3] Y. Ahn, S.J. Bae, M. Kim, S.K. Cho, S. Baik, J.I. Lee, J.E. Cha, Review of supercritical CO_2 power cycle technology and current status of research and development, Nucl. Eng. Technol. 47 (6) (2015) 647-661. https://doi.org/10.1016/j.net.2015.06.009.

[4] S. Liao, T. Zhao, Measurements of heat transfer coefficients from supercritical carbon dioxide flowing in horizontal mini/micro channels, J. Heat Transf. 124 (2002) 413-420. https://doi.org/10.1115/1.1423906.

[5] H. Li, A. Kruizenga, M. Anderson, M. Corradini, Y. Luo, H. Wang, H. Li, Development of a new forced convection heat transfer correlation for CO_2 in both heating and cooling modes at supercritical pressures, Int. J. Therm. Sci. 50 (12) (2011) 2430-2442. https://doi.org/10.1115/1.1423906.

[6] Z. Du, W. Lin, A. Gu, Numerical investigation of cooling heat transfer to supercritical CO_2 in a horizontal circular tube, J. Supercrit. Fluids 55 (1) (2010) 116-121. https://doi.org/10.1016/j.supflu.2010.05.023.

[7] C. Dang, E. Hihara, In-tube cooling heat transfer of supercritical carbon dioxide. Part 1. Experimental measurement, Int. J. Refrig. 27 (7) (2004) 736-747. https://doi.org/10.1016/j.ijrefrig.2004.04.018.

[8] C. Dang, E. Hihara, In-tube cooling heat transfer of supercritical carbon dioxide. Part 2. Comparison of numerical calculation with different turbulence models, Int. J. Refrig. 27 (7) (2004) 748-760. https://doi.org/ 10.1016/j.ijrefrig.2004.04.017.

[9] M. Xiang, J. Guo, X. Huai, X. Cui, Thermal analysis of supercritical pressure CO_2 in horizontal tubes under cooling condition, J. Supercrit. Fluids 130 (2017) 389-398. https://doi.org/10.1016/j.supflu.2017.04.009.

[10] H. Zhang, J. Guo, X. Huai, X. Cui, Thermodynamic performance analysis of supercritical pressure CO_2 in tubes, Int. J. Therm. Sci. 146 (2019) 106102. https://doi.org/10.1016/j.ijthermalsci.2019.106102.

[11] J. Guo, M, Xiang, H. Zhang, X. Huai, K. Cheng, X. Cui, Thermal-hydraulic characteristics pf supercritical pressure CO_2 in vertical tubes under cooling and heating conditions, Energy 170 (2019) 1067-1081. https://doi.org/10.1016/j.energy.2018.12.177.

[12] C. Huang, W. Cai, Y. Wang, Y. Liu, B. Li, Review on the characteristics of flow and heat transfer in Printed Circuit Heat Exchangers, Appl. Therm. Eng. 153 (2019) 190-205. https://doi.org/10.1016/j.applthermaleng.2019.02.131.

[13] S. Jeon, Y.J. Baik, C. Byon, W. Kim, Thermal performance of heterogeneous PCHE for supercritical CO_2 energy cycle, Int. J. Heat Mass Transf. 102 (2016) 867-876. https://doi.org/10.1016/j.ijheatmasstransfer.2016.06.091.

[14] W. Kim, Y.J. Baik, S. Jeon, D. Jeon, C. Byon, A mathematical correlation for predicting the thermal performance of cross, parallel, and counterflow PCHEs, Int. J. Heat Mass Transf. 106 (2017) 1294-1302. https://doi.org/10.1016/j.ijheatmasstransfer.2016.10.110.

[15] H. Zhang, J. Guo, X. Huai, K Cheng, X. Cui, Studies on the thermal-hydraulic performance of zigzag channel with supercritical pressure CO_2, J. Supercrit. Fluids 148 (2019) 104-115. https://doi.org/10.1016/j.supflu.2019.03.003.

[16] J.H. Kim, S. Baek, S. Jeong, J. Junge, Hydraulic performance of a microchannel PCHE, Appl. Therm. Eng. 30 (14-15) (2010) 2157-2162. https://doi.org/10.1016/j.applthermaleng.2010.05.028.

[17] X. Cui, J. Guo, X. Huai, H. Zhang, K. Cheng, J. Zhou, Numerical investigations on serpentine channel for supercritical CO_2 recuperator, Energy 172 (2019) 517-530. https://doi.org/10.1016/j.energy.2019.01.148.

[18] T.L. Ngo, Y. Kato, K. Nikitin, N. Tsuzuki, New printed circuit heat exchanger with S-shaped fins for hot water supplier, Exp. Therm. Fluid Sci. 30 (8) (2006) 811-819. https://doi.org/10.1016/j.expthermflusci.2006.03.010.

[19] T.L. Ngo, Y. Kato, K. Nikitin, T. Ishizuka, Heat transfer and pressure drop correlations of microchannel heat exchangers with S-shaped and zigzag fins for carbon dioxide cycles, Exp. Therm. Fluid Sci. 32 (2) (2008) 560-570. https://doi.org/10.1016/j.expthermflusci.2007.06.006.

[20] D.E. Kim, M.H. Kim, J.E. Cha, S.O. Kim, Numerical investigation on thermal–hydraulic performance of new printed circuit heat exchanger model, Nucl. Eng. Des. 238 (12) (2008) 3269-3276. https://doi.org/10.1016/j.nucengdes.2008.08.002.

[21] F. Chen, L. Zhang, X. Huai, J. Li, H. Zhang, Z. Liu, Comprehensive performance comparison of airfoil fins PCHEs with NACA 00XX series airfoil, Nucl. Eng. Des. 315 (2017) 42-50. https://doi.org/10.1016/j.nucengdes.2017.02.014.

[22] X. Xu, T. Ma, L. Li, Z. Min, Y. Chen, Y. Huang, Q. Wang, Optimization of fins arrangement and channel configuration in an airfoil fins PCHE for supercritical CO_2 cycle, Appl. Therm. Eng. 70 (1) (2014) 867-875. https://doi.org/10.1016/j.applthermaleng.2014.05.040.

[23] X. Cui, J. Guo, X. Huai, K. Cheng, H. Zhang, M. Xiang, Numerical study on novel airfoil fins for printed circuit heat exchanger using supercritical CO_2, Int. J. Heat Mass Transf. 121 (2018) 354-366. https://doi.org/10.1016/j.ijheatmasstransfer.2018.01.015.

[24] H. Zhang, J. Guo, X. Cui, J. Zhou, X. Huai, H. Zhang, K. Cheng, Z. Han, Experimental and numerical investigations of thermal-hydraulic characteristics in a novel airfoil fins heat exchanger, Int. J. Heat Mass Transf. 175 (2021) 121333. https://doi.org/10.1016/j.ijheatmasstransfer.2021.121333.

[25] Z. Guo, S. Zhou, Z. Li, L. Chen, Theoretical analysis and experimental confirmation of the uniformity principle of temperature difference field in heat exchanger, Int. J. Heat Mass Transf. 45 (2002) 2119-2127. https://doi.org/10.1016/S0017-9310(01)00297-6.

[26] H. Li, Y. Zhang, L. Zhang, M. Yao, A. Kruizenga, M. Anderson, PDF-based modeling on the turbulent convection heat transfer of supercritical CO_2 in the printed circuit heat exchangers for the supercritical CO_2 Brayton cycle, Int. J. Heat Mass Transf. 98 (2016) 204-218. https://doi.org/10.1016/j.ijheatmasstransfer.2016.03.001.

[27] F.R. Menter, Two-equation eddy-viscosity turbulence models for engineering applications, AIAA J. 32 (8) (1994) 1598–1605. https://doi.org/10.2514/3.12149.

[28] E.W. Lemmon, M.L. Huber, M.O. Mclinden, NIST Standard Reference Database 23: Reference Fluid Thermodynamic and Transport Properties (REFPROP), Version 9.0. (2010). http://www.mendeley.com/research/nist-standard-reference-database-23-reference-fluid thermodynamic-transport-properties-refpropversi/%5Cnhttp://www.nist.gov/srd/upload/REFPROP9.pdf.

[29] H. Zhang, J. Guo, X. Cui, X. Huai, Performance analysis of supercritical pressure CO_2 in several enhanced tubes with non-uniform heat flux, Appl. Therm. Eng. 180 (2020) 115823. https://doi.org/10.1016/j.applthermaleng.2020.115823.

[30] T.H. Kim, J.G. Kwon, S.H. Yoon, H.S. Park, M.H. Kim, J.E. Cha, Numerical analysis of air-foil shaped fins performance in printed circuit heat exchanger in a supercritical carbon dioxide power cycle, Nucl. Eng. Des. 288 (2015) 110-118. https://doi.org/10.1016/j.nucengdes.2015.03.013.

[31] Z. Han, J. Guo, H. Zhang, J. Chen, X. Huai, X. Cui, Experimental and numerical studies on novel airfoil fins heat exchanger in flue gas heat recovery system, Appl. Therm. Eng. 192 (2021) 116939. https://doi.org/10.1016/j.applthermaleng.2021.116939.

[32] X. Li, T. Deng, T. Ma, H. Ke, Q. Wang, A new evaluation method for overall heat transfer performance of supercritical carbon dioxide in a printed circuit heat exchanger, Energy Convers. Manage. 193 (2019) 99-105. https://doi.org/10.1016/j.enconman.2019.04.061.

[33] Z. Guo, W. Tao, R.K. Shah, The field synergy (coordination) principle and its applications in enhancing single phase convective heat transfer, Int. J. Heat Mass Transf. 48 (2005) 1797-1807. https://doi.org/10.1016/j.ijheatmasstransfer.2004.11.007.

[34] Y. Tao, Y. He, J. Huang, Z. Wu, W. Tao, Three-dimensional numerical study of wavy fins-and-tube heat exchangers and field synergy principle analysis, Int. J. Heat Mass Transf. 50 (2007) 1163-1175. https://doi.org/10.1016/j.ijheatmasstransfer.2006.03.019.

[35] Y. Tao, Y. He, J. Huang, Z. Wu, W. Tao, Three-dimensional numerical study and field synergy principle analysis of wavy fins heat exchangers with elliptic tubes, Int. J. Heat Fluid Flow 28 (2007) 1531-1544. https://doi.org/10.1016/j.ijheatfluidflow.2007.02.001.

[36] Y. He, W. Tao, F. Song, W. Zhang, Three-dimensional numerical study of heat transfer characteristics of plain plate fins-and-tube heat exchangers from view point of field synergy principle, Int. J. Heat Fluid Flow 26 (2005) 459-473. https://doi.org/10.1016/j.ijheatfluidflow.2004.11.003.

[37] W. Liu, Z. Liu, Z. Ming, Z. Guo, Physical quantity synergy in laminar flow field and its application in heat transfer enhancement, Int. J. Heat Mass Transf. 52 (2009) 4669-4672.

https://doi.org/10.1016/j.ijheatmasstransfer.2009.02.018.

[38] A. Bejian, Entropy Generation through Heat and Fluid Flow, Wiley, 1982.

[39] J.E. Hesselgreaves, Rationalisation of second law analysis of heat exchangers, Int. J. Heat Mass Transf. 43 (2000) 4189-4204. https://doi.org/10.1016/S0017-9310(99)00364-6.